Rational Design of Engineered Multifunctional Heterogeneous Catalysts. The Role of Advanced EPR Techniques

Morra, Elena; Maurelli, Sara; Chiesa, Mario; Giamello, Elio. Rational Design of Engineered Multifunctional Heterogeneous Catalysts. The Role of Advanced EPR Techniques. TOPICS IN CATALYSIS. 58 (12-13) pp: 783-795.
DOI: 10.1007/s11244-015-0418-5

Rational Design of Engineered Multifunctional Heterogeneous Catalysts. The Role of Advanced EPR Techniques.

Elena Morra,[1,2] Sara Maurelli,[1] Mario Chiesa,[1]* Elio Giamello[1]

Department of Chemistry, University of Torino, Via Giuria, 7 - 10125 Torino, Italy

Dutch Polymer Institute (DPI), P.O. Box 902, 5600 AX Eindhoven, The Netherlands

e-mail: mario.chiesa@unito.it

Abstract

The importance of surface paramagnetic species owes much to that of surface phenomena which are involved in numerous areas of chemistry and material science such as heterogeneous catalysis, photochemistry and, in general terms, nano-sciences and technology. In the present contribution the opportunities offered by the use of EPR in the field of heterogeneous catalysis, with emphasis on the application of hyperfine techniques, will be illustrated taking as an example Ti-based catalytic materials. The reductive activation of framework titanium ions in the different materials and their sub-sequent reactivity towards NH_3 is followed, highlighting subtle differences in chemical reactivity related to the different matrixes.

1. Introduction

Shifting from a trial and error to a rational approach based on the fundamental mechanistic understanding of structure property relationships is a strategic goal for both modern catalysis industry and academic researchers.

The establishment of a structure-activity-selectivity relationship for heterogeneous catalysts is particularly demanding and much more difficult to obtain compared to the homogeneous analogs. The heterogeneity of the support, the plurality and low concentration of the active surface sites, combined with difficulties in investigating the catalysts under reaction conditions, are just few examples of the challenges that need to be faced in order to achieve a proper understanding of the catalytic sites and, consequently, the rational design of the desired catalyst. Whatever the characterization techniques used for the investigation of the active sites, they should be very sensitive, able to discriminate between active and spectator species and versatile enough to work under conditions as close as possible to the reaction ones.

Electron Paramagnetic Resonance (EPR) techniques comply with most of these requirements with a main limitation, they are restricted to paramagnetic species only. Although this is a clear limitation in comparison to common techniques such as X-ray diffraction, vibrational or optical spectroscopy, there exists a wide variety of heterogeneous catalytic systems in which paramagnetic species are involved. Moreover, if it can be established that a paramagnetic entity is of importance within the catalytic cycle, EPR allows focusing exclusively on such a species, avoiding the inherent complexity associated to spectroscopically active spectator (diamagnetic) species.

Unpaired electrons associated to surface localized chemical entities such as transition metal ions (TMIs) are often involved in the formation of temporary chemical bonds with the reacting molecules, leading to specific activated complexes or reaction intermediates. Similarly, highly reactive molecules containing one or more broken bonds can be stabilized on surfaces or within porous media such as molecular sieves. These stabilized molecules, which are often paramagnetic, offer the possibility of controlled reactions with other molecules to produce specific products, whereas the corresponding gas phase reaction would not be as selective.

These considerations suggest that EPR spectroscopy, with its ability to detect small concentrations of paramagnetic species and to probe in detail those features of their electronic structure associated to the unpaired electron spin distribution, is a useful method of investigating heterogeneous catalysts and systems involving surfaces in general. A number of review papers have dealt with the subject since the pioneering applications of EPR to heterogeneous catalysis in the Sixties up to recent *in-situ* studies.[1,2,3,4,5,6,7] The potential of EPR in the characterization of paramagnetic solid surfaces and interfaces can be enormously extended by exploiting advanced pulse methods, which have successfully been employed in the characterization of biochemical systems, but are still of limited application in the field of heterogeneous catalysis and surface chemistry.[8] A review on the advantages of high field ENDOR in the characterization of functional sites in microporous materials can be found in ref.9, while some case studies are reported in ref 10. Even though the application of these techniques is limited to cryogenic temperatures and, at present, not applicable under *operando* conditions, so-called hyperfine spectroscopy (ESEEM, ENDOR, HYSCORE) allows monitoring the distribution of the unpaired electrons wave function, which is one of the most useful of the molecular “fingerprints” obtained from an EPR spectrum, over first and second coordinative shells. The link between coordination geometry and catalytic activity

further emphasizes the notion that a profound knowledge of the precise nature of the active site at the molecular level is of fundamental importance in the design of highly active catalysts, and synthetic factors that provoke even a subtle modification to the nature of the active site at the atomic scale deserve a thorough investigation.

The present paper offers a survey of recent and new results from our laboratory on the application of continuous wave (CW) and pulse EPR methods in order to answer specific questions inherent with the structure, distribution and reactivity of TMI species inserted in the framework of various inorganic microporous framework solids. In particular, the chemistry of titanium ions incorporated in two different silicate materials,TS-1 and ETS-10, featuring tetrahedrally and octahedrally coordinated titanium ions respectively and in alumino-phosphate materials with tetrahedrally coordinated ions (Figure1), will be covered as it provides a prototypical example of the potential of hyperfine techniques applied to the characterization of heterogeneous catalytic materials.

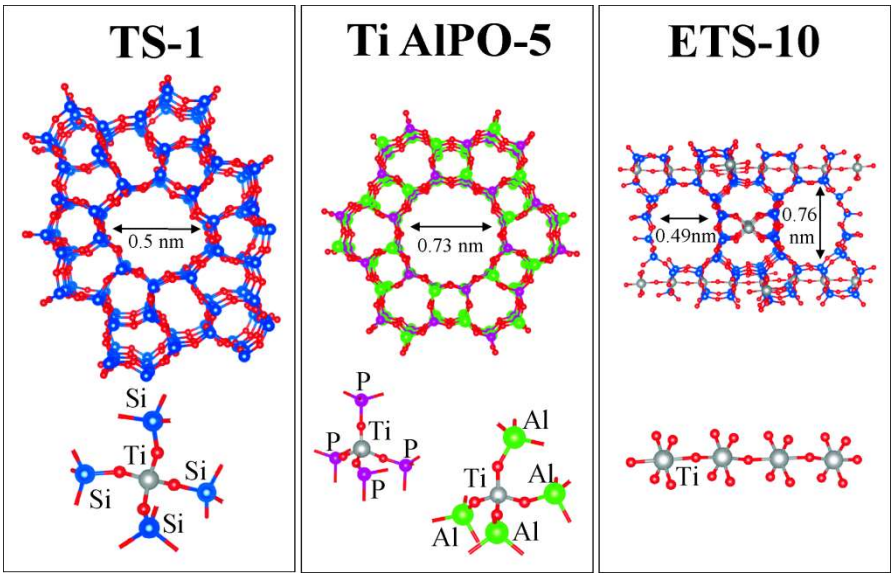

Figure 1. Architectures and titanium active sites of the microporous framework solids discussed. Oxygen ions are not labeled.

Titanium ions incorporated in the frame of silicate or porous aluminum phosphate materials provide an excellent example of so called “single site” catalysts. A ‘‘single-site’’ (catalytically active center) may consist of one or more atoms spatially isolated from one another, each site featuring a particular catalytic function.[11]An often drawn analogy is that with the complex design of multifunctional active sites within metallo-enzymes and the efficacy of the three-dimensional protein framework in facilitating highly selective and specific reaction pathways. Synthetic chemists have utilized the knowledge gained from

enzymatic active sites to develop porous inorganic frameworks, such as zeolites, to make active and selective catalysts for industrial processing.

The ways by which active dopant ions are introduced into a zeotype framework is fairly well understood and consist of two primary mechanisms. The first is the incorporation of charge-balancing cations, the second is the isomorphous substitution, whereby heteroatoms replace silicon atoms within the solid porous architecture. Arguably, the most well-known example from the past decade that successfully demonstrates the advantages that such a strategy could deliver, both from an academic and industrial perspective, relates to the silicalite family, and specifically to the titanium silicate, TS-1.[12]In this system, a small percentage of the Si(IV) ions in the silicalite framework (MFI) have been replaced with Ti(IV) ions. Therefore, instead of $Si(OSi)_4$, a $Ti(OSi)_4$ species exists, acting as an isolated metal-active center (Figure 1). Given the isoionic nature of the substituent, a charge imbalance does not occur from this substitution, and subsequently charge-balancing cations are not required. Instead, the active site is intimately incorporated into the pore walls of the MFI framework and securely located within the porous cavity, resulting in a material where the exchange of molecular ions is not readily feasible. A further advantage is that the substituted species can be stabilized into an energetically unfavorable geometry, with the possibility of becoming coordinatively unsaturated and enhancing the catalytic activity. Despite these advantages, comparatively few examples of isomorphous substitution in zeolite species exist owing to the stringent restrictions that are imposed on the ions (*i.e.* compatible charge and ionic size).

In 1982 a class of microporous materials, alumino-phosphates (AlPOs), were discovered, where isomorphous substitution of heteroatoms was readily plausible and is now commonplace.[13] Porous alumino-phosphate architectures, (AlPO-*n*), where *n* denotes a particular structure type, represent a class of microporous crystalline materials that are akin to the well-known zeolites and characterized by neutral lattices constituted by alternating PO_4 and AlO_4tetrahedra. Their uniform and molecular sized pores can be specifically tailored towards shape-selectivity for various catalytic transformations.[14]Beside their structural features, the chemical reactivity of these materials can be suitably modified by the isomorphous incorporation of various transition metal ions (TMIs). Titanium insertion in tetrahedral sites of AlPO materials has been found particularly effective in enabling catalysts with superior conversions and selectivities in many important reactions,[14,15,16,17] the catalytic activity being associated to the coordinatively unsaturated tetrahedral Ti(IV) ions.[18,19,20,21,22] Despite the structural analogy, AlPOs show a greater

flexibility than silicalite toward chemical substitution, as shown by the large number of different incorporating TMIs which confer to these materials a peculiar bi-functional character due to the simultaneous presence of Brønsted and redox sites with great potential for application in catalytic processes.[23] A comparison between tetrahedral Ti ions in the frame of the zeolite TS-1 and in TiAlPO is therefore particularly interesting also in light of the huge amount of experimental and theoretical results on the structure and reactivity of tetrahedral Ti sites in zeolite TS-1,[24,25] allowing to study the influence of the matrix [26] on the chemistry of isolated TMIs in well-defined environment.

TS-1 and TiAlPO-5 are representative of the large class of microporous framework solids, which contain tetrahedrally coordianted metal atoms.

In 1989 a family of microporous titanosilicates (generically denoted ETS) was discovered, in which the metal ions (Ti^{4+}) are octahedrally coordinated.[27] ETS-10, one of the members of this family, has been proven to be an effective catalyst for various reactions,[28] however the most interesting featurethat makes ETS-10 a unique material is that it contains periodicallypositioned quantum wires [-O-Ti(O-)$_4$-O-] with a diameter(*d*) of ~0.7 nm running along the two perpendicular directionsin the crystal (Figure 1).[29]By analogy with the case of tetrahedral systems, we have investigatedthe possibility of creating reduced Ti^{3+} states in the-OTiOTiO- quantum wires, taking advantage of the factthat, due to the microporous structure of this zeolitic material,the Ti chains have surface character andcan easily interact with adsorbates.The reduction has been achieved by contacting the previously evacuated zeolitic material with triethylaluminum (TEA)vapors. It will be shown that this experimentalapproach does indeed produce nonstoichiometric-OTiOTiO- wires (containing Ti^{3+} ions), whose propertiescan be usefully compared with those of reduced TS-1 and TiAlPO-5 as well as to reduced TiO_2 andTi_2O_3.[30]

2. Materials and Methods.

2.1 Sample preparation

The TS-1 sample prepared by ENI (Instituto G. Donegani, Novara, Italy) and sodium form of ETS-10 prepared by Engelhard (Iselin, NJ, USA) were fully characterized elsewhere.[25,29,31,32] In the case of TS-1 the Ti loading was 2.98 wt%, as determined by the cell volume expansion, and the absence of extra phases of TiO_2 was carefully checked.

For the spectroscopic characterization, the calcined samples were loaded into quartz tubular cells that allowed in situ EPR measurements and evacuated to a final pressure of 10^{-5} mbar at 673 K to obtain dehydrated samples. Triethylaluminum (TEA) (Aldrich) was purified by the freeze-pump-thaw method and delivered on the outgassed samples by the gas phase.

TiAlPO-5 was prepared by hydrothermal synthesis as described elsewhere.[33] Calcined samples were dehydrated under vacuum by gradually raising the temperature to T = 673 K over a period of 2 h and kept at that temperature for 1 h. The dehydrated samples were then reduced under 100 Torr of H_2 at T = 673 K.

To prepare Ti^{3+}-ammonia complexes, ammonia (20 mbar) was delivered on the activated sample at room temperature.

2.2 EPR characterization

X-band CW EPR spectra were detected at 77 K on a Bruker EMX spectrometer (microwave frequency 9.75 GHz) equipped with a cylindrical cavity. A microwave power of 10 mW, a modulation amplitude of 0.3 mT and a modulation frequency of 100 KHz were used. Pulse EPR experiments at X-band (9.76 GHz) and Q-band (34 GHz) were performed on an ELEXYS 580 and SuperQ FT-EPR Bruker spectrometer equipped with a liquid-helium cryostat from Oxford Inc. The magnetic field was measured by means of a Bruker ER035 M NMR gauss meter.

Electron-spin-echo (ESE) detected EPR experiments were carried out with the pulse sequence: $\pi/2–\tau–\pi–\tau–echo$. At X-band microwave pulse lengths $t_{\pi/2}$ = 16 ns and t_π = 32 ns and a τ value of 200 ns were used. Q-band conditions were as follows: $t_{\pi/2}$ = 20 ns and t_π = 40 ns and a τ value of 200 ns. A 1 kHz repetition rate was used at both X- and Q-band frequencies. Further experimental details are specified in the figure captions.

Hyperfine Sublevel Correlation (HYSCORE) experiments[34] were carried out with the pulse sequence $\pi/2–\tau–\pi/2–t_1–\pi–t_2–\pi/2–\tau–echo$. At X-band the microwave pulse length $t_{\pi/2}$ = 16 ns and t_π = 16 ns were adopted. The time intervals t_1 and t_2 were varied in steps of 8 ns starting from 96 ns to 2704 ns. In order to avoid blind spot effects different τ values were chosen, which are specified in the figure captions. At Q-band the following parameters were used: microwave pulses of lengths $t_{\pi/2}$ = 20 ns, t_π = 40 ns, starting times 100 ns for t_1 and t_2, and time increments $\Delta\tau$ = 8 ns (data matrix 200 × 200). Spectra with

different τ values, specified in the figure captions, were recorded. The temperature adopted for the experiments is specified in the figure captions. A shot repetition rate of 1.25 kHz was used at both X- and Q-band frequencies. A four-step phase cycle was used for eliminating unwanted echoes. The time traces of the HYSCORE spectra were baseline corrected with a third-order polynomial, apodized with a Hamming window and zero filled. After two dimensional Fourier transformation, the absolute value spectra were calculated. The spectra were added for the different τ values in order to eliminate blind-spot effects. EPR and HYSCORE spectra were simulated using the Easyspin software.[35] In the HYSCORE simulations an excitation width of 80 MHz was assumed, compatible with the 16 ns and 20 ns $\pi/2$ pulse length used in X- and Q-band experiments.

3. Isomorphous Substitution of Titanium in Open Framework Materials.

3.1 Tetrahedrally Coordinated Titanium Ions in SilicaliteTS-1 and TiAlPO-5

The incorporation of transition metal ions (TMI) in the framework of micro and mesoporous materials generates isolated sites that often lack structural precedent in molecular chemistry. These active metal centers give rise to a formidable variety of processes and exert different functionalities, which are critically modulated by the nature of the surrounding ligands, the local coordination geometry and the specific oxidation states. Prototypical examples are provided by the incorporation of Ti ions in the framework of Silicalite 1 (TS-1) and aluminum phosphate materials (AlPOs). The distinctive feature of TS-1 is the presence of isolated Ti ions forced to assume an unusual tetrahedral coordination by insertion in the rigid framework of the solid, which primes the diluted metal centers for the remarkable inner-sphere redox reactivity of TS-1.Ti^{4+} sites in TS-1 have been the object of intense and detailed characterization from both the experimental and theoretical point of view[25]and consensus has been reached in establishing that Ti is preferentially located inside a tetrapodalstructure.[32]The application of EPR requires that paramagnetic species (Ti^{3+} ions) are generated, which offers the opportunity to study the redox chemistry of these solids. EPR studies have been reported in the past to probe the nature of Ti^{3+}species in TS-1, however clear evidence of tetrahedrally coordinated Ti^{3+} ions was only obtained upon irradiation of the solid under ionizing radiations,[36] while chemical reduction led to spectra amenable to distorted octahedral coordination, likely due to reduction of extra framework TiO_2 impurity phases. We recently found that reaction of TS-

1 with aluminum alkyl compounds such as TEA leads to the reduction of framework Ti^{4+}ions and the formation of Ti^{3+}ions.[37]

Upon contacting the diamagnetic solid with TEA vapors an intense EPR spectrum with pseudo-axial symmetry is observed (Figure 2a). Computer simulation (Figure 2a and Table 1) shows that the spectral profile is dominated by a species (S1) with slightly rhombic **g** tensor (g_1 = 1.922, g_2 = 1.939, g_3 = 1.9897) with the contribution of a second species (S2 in Table 1) with maximum abundance of 10% due to Ti^{3+} species with a different environment, either due to interactions with TEA residuals or to a non regular framework site position.

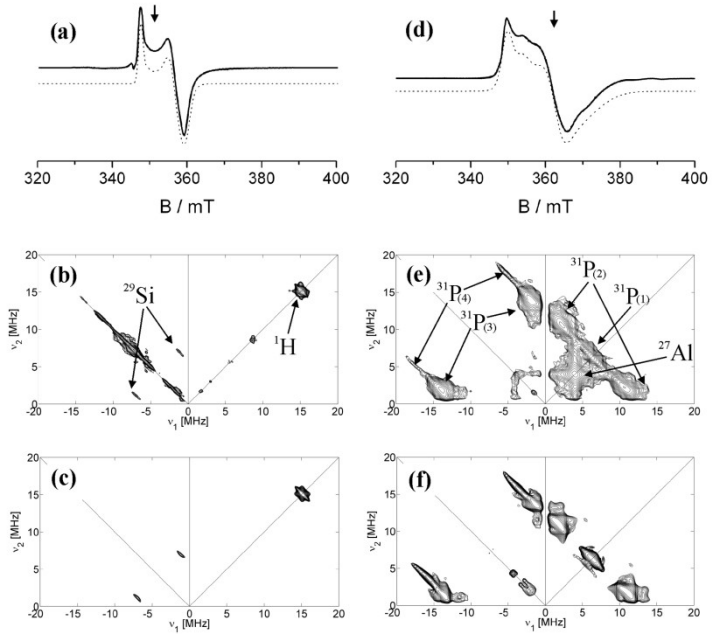

Figure 2. (a) Experimental (solid line) and simulated (dotted line) X-band CW-EPR spectrum of Ti^{3+} species generated in TS-1 upon reaction with TEA; (b) Experimental HYSCORE spectrum of reduced TS-1 recorded at a magnetic field position corresponding to the arrow in spectrum (a) and τ value 208ns; (c) Computer simulation of the ^{1}H and ^{29}Si signals of the experimental HYSCORE spectrum in (b); (d) Experimental (solid line) and simulated (dotted line) X-band CW-EPR spectrum of Ti^{3+} species generated in TiAlPO-5 upon reaction with H_2 at 673 K; e) Experimental HYSCORE spectrum of reduced TiAlPO-5 recorded at a magnetic field position corresponding to the arrow in spectrum (c); (f) Computer simulation of the ^{31}P signals of the experimental HYSCORE spectrum in (e). In both experimental and simulated spectra three τ values (104, 136, and 250 ns) were summed together after Fourier transform to avoid blind spots. CW EPR spectra were recorded at T = 77 K, while HYSCORE spectra at T = 10 K. The simulated HYSCORE spectra were obtained with the spin Hamiltonian parameters reported in Table 1.

The free-ion ground state of a $3d^1$ spin system, such as Ti^{3+}, may be split by a cubic crystalline field.[38,39] In these circumstances, the *g* values for the ground state critically depend upon the strength and symmetry of the local crystal field. When Ti^{3+} is subjected to a perfect cubic crystalline field from tetrahedral or octahedral coordination, its 5-fold orbital

degeneracy is split into two and three degenerate levels. In a tetrahedral field the doublet has lower energy, whereas in an octahedral field the reverse is true. In both cases a distortion from perfect cubic symmetry is expected for a $3d^1$ system in order to explain the experimentally observed anisotropy of the EPR signal. In the classical crystal-field theory, the EPR parameters are explained by using the perturbation formulas based on the one-spin-orbit (SO)-parameter model.[40] In the simple case of an axial symmetry the theoretical expressions for g values calculated to first order are[39] $g_{\|}\approx g_e$ and $g_{\perp}\approx g_e - 6\lambda/\Delta$, where g_e is the free electron g value (2.0023), Δ is the energy gap between the ground state and excited levels and λ the Ti spin orbit coupling constant ($\approx$ 154 cm^{-1}).[38]The g factors are consistent with those reported for Ti^{3+} defect centers, where Ti^{3+} ions substitute for the tetrahedral Si^{4+} site of beryl crystals[41] and strongly indicates the formation of framework Ti^{3+} ions in tetrahedral coordination upon reaction of the dehydrated sample with TEA vapors. In order to confirm this analysis and to ascertain the local coordination environment of the formed Ti^{3+} species, HYSCORE experiments have been performed. Figure 2b shows the HYSCORE spectrum of the TS-1 reduced sample.

Table 1. Spin Hamiltonian parameters for the different Ti^{3+} species described. All hyperfine coupling constants are given in MHz.

System		g_1	g_2	g_3		A_1	A_2	A_3	ρ(3s) (%)
TS-1	S1	1.922±0.001	1.939±0.001	1.9897±0.0002	^{29}Si	±6.8±0.2	±7.1±0.2	±10.0±0.2	0.20
	S2	1.91±0.01	1.960±0.005	1.981±0.002		±0.3±0.3	±0.3±0.3	∓1.6±0.4	0.008
TiAlPO-5	S1	1.898±0.005	1.918±0.005	1.991±0.002	^{31}P	±17.0±0.5	±16.0±0.5	±25.0±0.5	0.20
						±12.9±0.5	±11.9±0.5	±15.9±0.5	0.14
	S2	1.90±0.01	1.90±0.01	1.969±0.002		±9.0±0.5	±7.0±0.5	±12.0±0.5	0.09
						±1.0±0.5	±1.0±0.5	±3.0±0.5	0.017
ETS-10	S1	1.915±0.005	1.947±0.005	1.974±0.005	^{29}Si	±8±2	±8±2	±14±1	0.25
					^{27}Al	±4±2	±3±2	±9±1	0.16
	S2	1.74±0.02	1.87±0.02	1.87±0.02					

The spectrum is characterized by the presence in the (-,+) quadrant of a pair of cross peaks centered at about (-0.92, +6.62) MHz and (-6.62, +0.92) MHz which are unambiguously assigned to (relatively) strongly coupled ^{29}Si in the surrounding of the Ti^{3+} center. The signal intensity is relatively low according to the low natural abundance of ^{29}Si (4.67%). The elongated shape of the cross peaks indicates a relatively large anisotropy. A weak ridge with maximum extension of approximately 2.0 MHz and centered at the ^{29}Si Larmor frequency was also observed in the (+,+) quadrant at other magnetic field settings (see ref 37).Finally, centered at the ^{1}H nuclear Larmor frequency a small ridge with

maximum extension of approximately 2.5 MHz is present. The presence of a proton is necessary for the sake of charge compensation, however, the ridge extension is much smaller than what observed in the case of protons in the Ti^{3+} first coordination sphere[42] indicating that the proton does not belong to an OH^- group in the proximity of the Ti^{3+}centre. A possible reaction pathway, accounting for the Ti reduction assisted by TEA, may be the formation of an alcoholate of the form $[OCH_2CH_3]^-$ as discussed in ref. 37

The hyperfine coupling constant parameters were extracted by means of computer simulation of the experimental spectra and are listed in Table 1. The values for both set of nuclei compare nicely with those reported by Zamani et al.[43] in the case of VO^{2+} groups incorporated in mesoporous silica materials and together with the *g* factors of the CW-EPR spectrum (characteristic of a local tetrahedral symmetry) provide unique and direct evidence for the framework incorporation of the formed Ti^{3+} species as shown in Scheme 1a. We remark that this result is not trivial as, although the starting TS-1 material features framework incorporated Ti^{4+} ions, chemical reduction to Ti^{3+} not necessarily implies that the reduced species preserves its framework nature and local coordination symmetry.

The hyperfine tensors reported in Table 1 can be decomposed in the isotropic (Fermi contact) and anisotropic (dipolar) tensors, from which the spin density repartition in the Si 3*s* orbital can be estimated.

Considering a value of a_0 = -3995.33 MHz for unit spin density in the Si 3*s*orbital,[44] and including a correction for departure of the *g* value ($g_{iso}[Ti^{3+}/TS\text{-}1]$ = 1.950) from the free electron value (g_e= 2.0023) the spin population in the Si 3*s* orbital can be estimated from the following equation:

$$\rho_{Si(3s)} = \frac{A_{iso}}{a_0}\frac{g_e}{g_{iso}} \quad (1)$$

to be approximately 0.20% and 0.008% for the two cases. A negative sign is taken for both a_0 and A_{iso} due to negative sign of the ^{29}Si nuclear *g* factor (g_n=-1.11058). As discussed by different Authors in the case of similar systems,[45] the spin density transfer occurs via a through bond mechanism and is expected to depend markedly on bond angle and distance of the Ti-O-Si, making the Fermi contact term a sensitive structural probe and justifying significantly different coupling constants.

In the case of AlPOs materials, the reaction with TEA, described before, leads to disruption of the crystalline network, probably due to reduction of the P^{5+} ions. However, we found that Ti^{4+}, at variance with TS-1, is easily reducible by treatment under hydrogen atmosphere at 400°C. Upon this treatment the spectrum shown in Figure 2d is observed. Similarly to the previous case the spectrum is characterized by a nearly axial **g** tensor (Table 1). The exact line shape of the experimental EPR spectrum could only be reproduced in the simulation by adding a second species with lower abundance (about 35±5% as estimated from the computer simulation) and axial **g** tensor ($g_{||}$=1.969, $g_{\perp}$=1.90) suggesting that more than one Ti^{3+} species, differing in the local coordination geometry, are contributing to the overall ESR powder spectrum. The *g* values of both species are typical for Ti^{3+} in a tetrahedral crystal field. Comparison of the spectrum with that of TS-1 indicates a much broader line width arising from the superhyperfine interaction of Ti^{3+} with the magnetically active ^{31}P (*I*=1/2) and ^{27}Al (*I*=5/2) framework nuclei. These interactions are well resolved by means of HYSCORE experiments.[33]A representative spectrum is shown in Figure 2e. The spectrum is characterized by different pairs of cross peaks indicated with P(1)-P(4) which stem from the superhyperfine interaction between the unpaired electron of Ti^{3+} and different ^{31}P nuclei. Two sets of cross-peaks (P(1) and P(2)) appear in the (+,+) quadrant approximately centered around the ^{31}P nuclear Larmor frequency ($\nu(^{31}P)$ = 6.24 MHz). The first set (P(1)) is characterized by a ridge shape with maximum extension of about 3 MHz, while the second set (P(2)) appears at *ca*. (11.3, 1.8) (1.8, 11.3) MHz along the diagonal of the (+,+) quadrant. The other cross peaks (P(3) and P(4)) appear in the (-,+) quadrant separated by $2\nu(^{31}P)$ and positioned at approximately (-14.2, +2.1) (-2.1 +14.2) MHz and (-16.5, +4.1) (-4.1 +16.5). In the (+,+) quadrant a diagonal peak centered at the ^{27}Al nuclear Larmor frequency ($\nu(^{27}Al)$ = 4.02 MHz) is also present, which is due to remote (matrix) ^{27}Al nuclei. Similar HYSCORE spectra were observed at different magnetic fields across the EPR spectrum (also at the outer field settings where only one species is contributing), indicating that the different species, which contribute to the overall spectrum, share a similar phosphorous-rich local environment and that the observed differences in the **g** tensor may be due to small alterations in local coordination geometry. The ^{31}P HYSCORE spectra taken at different magnetic field positions could be well reproduced by simulation using four different ^{31}P nuclei with hyperfine parameters listed in Table 1, where a positive sign was assumed based on the positive ^{31}P nuclear *g* factor. As in the case of TS-1, such isotropic couplings are induced by spin density transfer to ^{31}P through the directly coordinated oxygen and are particularly

sensitive to structural variations, the values depending markedly on the M-O-P bond angle. The presence of large ^{31}P couplings typical for phosphate coordination in the HYSCORE spectrum, combined with the absence of such a coupling due to ^{27}Al provides thus a unique and direct proof for framework substitution of Ti^{3+} for the isovalent Al^{3+}. Noticeably, given the isoionic charge of Ti^{3+} and Al^{3+} no proton signals are observed in this case, as no charge compensation is needed (Scheme 1a). The spin density transfer over the nearby phosphorous ions can be estimated based upon Eq. 1 as done in the case of TS-1. Considering the value of a_0 = 10201.44 MHz for unit spin density on the ^{31}P 3*s* orbital and $g_{iso}[Ti^{3+}/TiAlPO\text{-}5]$ = 1.935,the corresponding spin density in the P 3*s* orbital varies in the range ≈ 0.20% - 0.017% in line with the case of Ti^{3+} inserted in the silica frame. The important difference to be highlighted between TS-1 and TiAlPO-5 is however the different reducibility of framework Ti in the two systems. Ti ions replacing for Al^{3+} framework AlPO-5 ions are easily reducible by virtue of the isoionicity of the two ions. This fact infers to TiAlPO-5 a much higher redox activity with respect to the case of Ti silicalite, which may be at the origin of the catalytic activity of TiAlPO-5 towards selective oxidation reactions using molecular oxygen as the oxidant.[46]We remark that only approximately 20% of the inserted Ti ions are redox active and located at Al^{3+} sites, the rest substituting for P framework sites.[32,33]

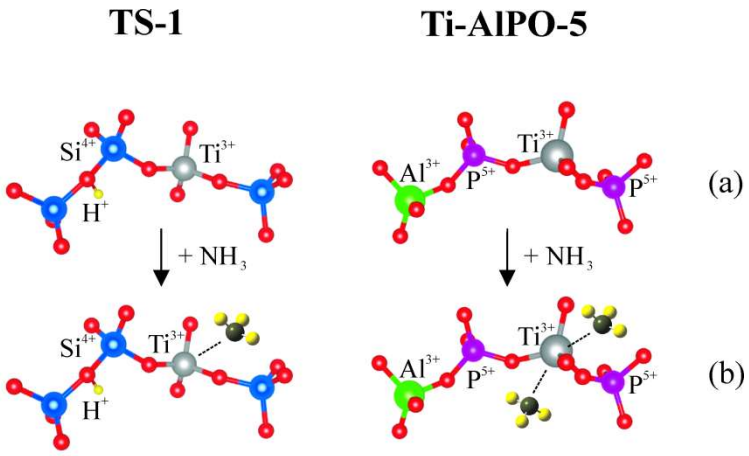

Scheme 1 Ti^{3+} coordination and local environment as deduced from HYSCORE experiments (see text).

3.2 *Reduced Ti species in ETS-10*

At variance with the previous cases, isomorphous substitution of Ti^{4+} in place of Si^{4+} in the framework of ETS-10 leads to six-fold coordinated Ti ions. ETS-10 is composed of octahedrally coordinated $TiO_{6/2}$ units and tetrahedrally coordinated $SiO_{4/2}$ units. The $TiO_{6/2}$

octahedra connect through the apical oxygen atoms forming linear chains of corner-sharing units surrounded by $SiO_{4/2}$ tetrahedra.[27b]The structure of ETS-10 is inherently disordered as the result of the intergrowth of two end polymorphs. The most remarkable feature of ETS-10 is however the presence of monoatomic-OTiOTiO- rows embedded into a highly insulating SiO_2 frame originated by corner sharing TiO_6^{8-}octahedra. These well-defined -OTiOTiO- chains behave as monoatomic quantum wires and have been studied in the past. Particularly interesting in this context is the possibility to inject excess electrons in the system in order to study the redox behavior and collective properties of the solid.[29d]

Upon reaction with TEA intense EPR spectra are observed characterized by a complex powder pattern strongly dependent on temperature and incident microwave power. Typical spectra are presented in Figure 3a-e, where the evolution of the spectrum as a function of temperature is shown. At room temperature the spectrum is characterized by a relatively narrow resonance absorption (S1 in Table 1) which starts to broaden below 80K.

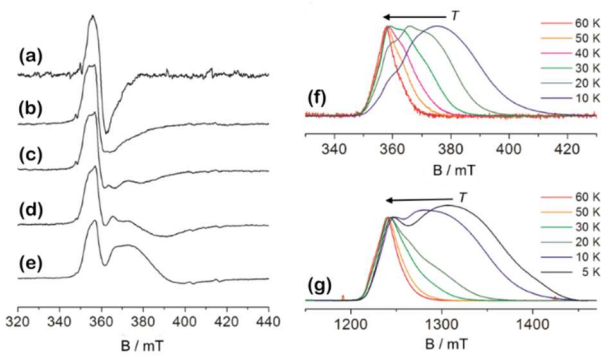

Figure 3. Representative field-swept EPR spectra of reduced ETS-10 recorded at different temperatures. On the left: X-band CW EPR spectra recorded respectively at temperature (a) 300 K, (b) 80 K, (c) 50 K, (d) 20 K and (e) 10 K. All spectra were recorded with 25 dB power attenuation except for spectrum (e) which was recorded at 35 dB attenuation. The attenuation was chosen in order to avoid saturation effects. On the right: ESE detected EPR spectra recorded at (f) X-band and (g) Q-band frequencies. All spectra are normalized.

At 20K (Figure 3d) a new species is observed resonating at higher magnetic field and characterized by a pseudo axial *g* symmetry with principal values $g_{||}$=1.74 and $g_{\perp}$=1.87. The evolution of the EPR spectrum as function of temperature can also be followed by echo detected EPR. Two pulse echo detected X-band and Q-band EPR spectra recorded at different temperatures are shown in Figures 3f and 3g respectively. The evolution of the spectra is consistent with the CW X-band behavior showing a progressive shift of the resonance absorption towards higher magnetic fields (lower *g* values) as the temperature decreases. The spin Hamiltonian parameters of the two species based on computer

simulation of the X- and Q-band experimental spectra are reported in Table 1. For species S2 the data refer to spectra recorded at T = 5 K.

In order to better characterize the nature of the two Ti^{3+} species HYSCORE experiments have been carried out to resolve hyperfine interactions with nearby magnetically active nuclei. Experiments have been performed at two different magnetic field settings corresponding to spectral regions where the overlap of species 1 and 2 is minimal.

The HYSCORE spectra recorded at X- and Q-band are shown in Figure 4.

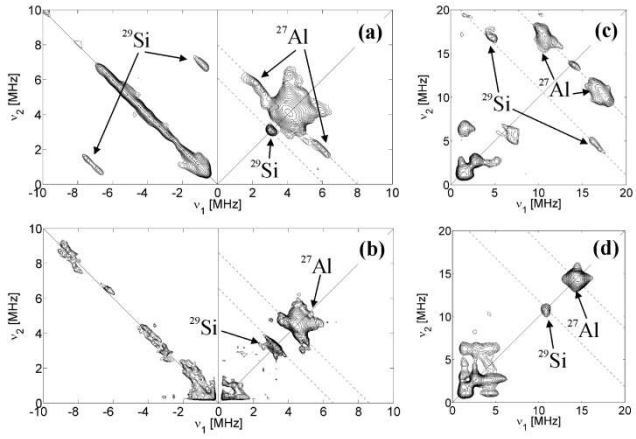

Figure 4. X-band HYSCORE spectra recorded at T = 10 K and τ = 208 ns at observer positions (a) 360.0 mT and (b) 388.0 mT. The contour level in (b) is 3 times lower than in (a) to ensure that no signals are missed. (c) Q-band HYSCORE spectrum recorded at T = 30 K at a magnetic field setting (1242.5 mT) corresponding to the observer position of Figure 4(a). (d) Q-band HYSCORE spectrum recorded at T = 10 K at a magnetic field setting (1290.0 mT) corresponding to the observer position of Figure 4(b). Q-band HYSCORE spectra were recorded at τ = 144 ns in order to suppress the contribution of remote ^{27}Al nuclei. The computer simulation of the HYSCORE spectrum (c) is shown as Supporting Information.

The HYSCORE spectrum recorded at a field position corresponding to the maximum absorption of species 1 (S1) is characterized by signals in both quadrants due to the interaction of the unpaired electron with ^{27}Al and ^{29}Si nuclei. In the (-,+) quadrant a pair of cross peaks centered at about (-0.83, +6.83) MHz and (-6.83, +0.83) MHz and separated by approximately $2\nu_{Si}$ are unambiguously assigned to (relatively) strongly coupled ^{29}Si in the surrounding of the Ti^{3+} centers similar to those observed in the case of TS-1. The signal intensity is relatively low, in line with the low natural abundance of ^{29}Si (4.67%). The elongated shape of the cross peaks indicates a relatively large anisotropy. The hyperfine coupling constant parameters were extracted by means of computer simulation of the experimental spectrum recorded at Q-band frequency (Figure 4c and Supporting Information) and are listed in Table 1, where the signs were chosen based on the point dipolar approximation and considering that $g_n(^{29}Si) < 0$. The values compare nicely with those obtained in the case of the reduced Ti silicalite TS-1, where Ti^{3+} ions are

incorporated in the siliceous framework in a tetrahedral symmetry. In the previous cases, the hyperfine tensors reported in Table 1 can be decomposed in the isotropic (Fermi contact) A_{iso}= -10 MHz and a dipolar component T = 2 MHz leading to a spin density in the Si 3*s* orbital of approximately 0.25% in good agreement with the case of TS-1, although slightly larger.

In addition to signals associated to ^{29}Si, HYSCORE spectra of reduced ETS-10, also show two cross peaks centered at the nuclear Larmor frequency of ^{27}Al at this field (13.825 MHz in Figure 4c).Simulation analysis indicates that the two cross peaks are best reproduced assuming an hyperfine tensor dominated by the Fermi contact interaction with A_{iso}= 5.3 MHz and a dipolar term T of the order of 1 MHz (Table 1). These values nicely correlates with values recently observed by some of us in the case of VO^{2+}-O-Al linkages in V doped alumino-phosphate materials.[47] Considerations analogous to those described in the case of Si allow inferring a spin density in the Al 3*s* orbital of the order of 0.16% consistent with the spin density transfer over the Si framework.

The observation of a relatively large hyperfine coupling indicates that Al^{3+} ions, released from TEA, are located in the proximity of the Ti^{3+} reduced ions acting as a charge compensating agent. We remark that such a situation was not observed in the case of TS-1. As an overall, species S1, characterized by a relatively small *g* anisotropy, displays distinct hyperfine couplings to Si and Al ions analogous to those observed for isolated Ti^{3+} or VO^{2+} in silica or alumino-phosphate frameworks.

A totally different scenario is displayed by species S2, characterized by a more pronounced ***g*** anisotropy and considerably lower *g* values. Most interestingly, X- and Q-band HYSCORE spectra recorded at a field position coinciding with species S2 (Figures 4b and 4d) reveal a very different situation, as all the large hyperfine couplings to ^{29}Si and ^{27}Al ions are disappeared. In particular for case of Al only signals stemming from matrix (remote) nuclei are observed, while for Si, a small ridge with maximum amplitude of approximately 1.2 MHz is present corresponding to a drop of the unpaired electron spin density in the Si 3*s* orbital of one order of magnitude. Absence of large couplings typical for isolated Ti^{3+} in silica framework (TS-1) strongly suggest that the unpaired electron spin density is delocalized over several nuclei even at cryogenic temperatures. Given the presence of 1D Ti-O-Ti chains comparison may be set to the class of low dimensional $3d^1$systems such as the Mott insulators TiOX (X=Cl,Br).[48] These systems are characterized by 1D antiferromagnetic spin S= 1/2 chains, showing transition to non

magnetic states at low temperatures (below 70 K). In our case we observe an increase of the spectral intensity on lowering the temperature, which indicates a Curie-like behavior incompatible with the presence of -Ti^{3+}-O-Ti^{3+}- structures. Similar structures, if present, are not expected to contribute to the EPR spectra at low temperature. A possible explanation is that reaction with TEA leads to only a partial reduction of the Ti ions in a row so that structures of the type -O-Ti^{3+}-O-Ti^{4+}-O- are present, whereby unpaired electrons are delocalized over larger portions of the frame, explaining the absence of large ^{29}Si couplings. This behavior would be consistent with the quantum wire behavior reported for ETS-10.

4. Mechanistic Insights into the Coordination Chemistry of Tetrahedral Ti(III): the Reactivity with NH_3 of reduced TS-1 and TiAlPO-5.

A key aspect in the study of potentially catalytically active species is the assessment of their chemical accessibility and reactivity. Tetrahedrally coordinated titanium ions are unsaturated and prone to coordinate incoming molecular species. In order to check for the reactivity of Ti^{3+} species formed by reduction of TS-1 and TiAlPO-5, we studied the coordination of ammonia. Adsorption of NH_3 at the active EPR site is expected to lead to a modification of the local crystal field experienced by the metal cation and this, in turn, is expected to have profound influence on the *g* factors of the EPR spectrum. Indeed upon adsorption of ammonia on both reduced TS-1 and TiAlPO-5 the features of the spectra reported in Figures 2a and 2d drastically change, giving rise to a new spectrum (Figures5a and 5d) dominated by a species whose *g* components are g_1 = 1.90, g_2 = 1.949, and g_3 = 1.965 (Table 2) typical for Ti^{3+} species characterized by a distorted octahedral field. In agreement with the slight heterogeneity of the EPR spectrum of reduced TS-1and TiAlPO-5, also in the case of ammonia adsorption, more species were needed to correctly reproduce the experimental spectral pattern.

The fine details of NH_3 coordination can be obtained by directly monitoring the ^{14}N superhyperfine intercations by means of HYSCORE spectroscopy. The HYSCORE spectrum of NH_3 adsorbed on the reduced TS-1 sample recorded at observer position 356.1 mT is reported in Figure 5b along with the corresponding computer simulation (Figure 5c). The spectrum is dominated in the (−,+) quadrant by a pair of cross-peaks centered at about (-3.5, 6.9) and (-6.9, 3.5) MHz, which are assigned to the double-quantum transitions (DQ) arising from the hyperfine interaction of the unpaired electron

with a nitrogen nucleus (I = 1). The HYSCORE spectrum of a S = 1/2, I = 1 disordered system is typically dominated by the cross peaks between the DQ frequencies[49]

$$\nu_{\mathrm{dq}}^{\alpha,\beta} = 2\sqrt{\left(\frac{a}{2} \pm \nu_I\right)^2 + K^2(3+\eta^2)} \qquad (2)$$

where a is the hyperfine coupling at a given observer position while $K = e^2qQ/4h$ is the quadrupolar coupling constant and η the so called asymmetry parameter. K and η are related to the principal values Q_x,Q_y and Q_z of the traceless **Q** tensor by the following relations: $Q_x = -K(1-\eta)$, $Q_y = -K(1+\eta)$ and $Q_z = 2K$. From Equation (2) and the position of the DQ cross-peaks, it can be derived a maximum hyperfine interaction of the order of 5 MHz and a quadrupole interaction of the order of 2-3 MHz. Similar spectra were observed upon adsorption of the same amount of ammonia on reduced TiAlPO-5 (Figure 5e). A noticeable difference is however the presence in this case of sum combination peaks of the form ($-2\nu_\beta^{DQ}$, $2\nu_\alpha^{DQ}$), which indicate that two nearly equivalent NH_3 molecules are coordinated to the same Ti^{3+} ion. Simulation of the spectrum (Figure 5f) was carried out considering a three spin system S=1/2, I_a=1 and I_b=1. Attention was paid not only to reproduce the shape of the DQ peaks, but also to fit the positions of the cross-peaks between the different single-quantum (SQ) frequencies and of the SQ-DQ cross-peaks (see arrows).

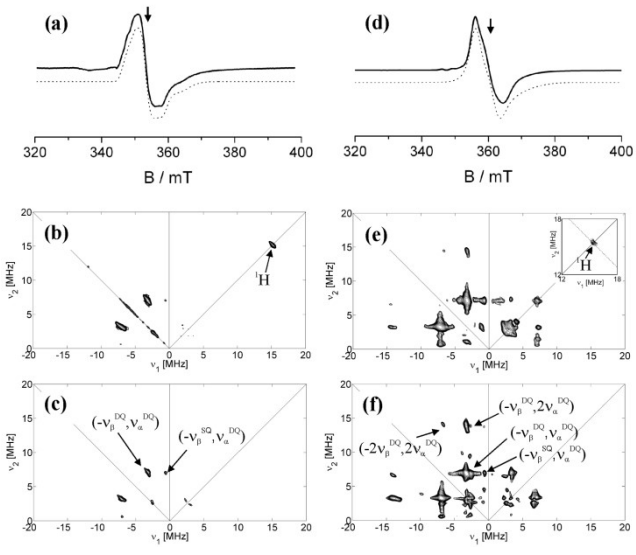

Figure 5. NH_3 adsorbed on reduced TS-1 and TiAlPO-5. (a) Experimental (solid line) and simulated (dotted line) X-band CW-EPR spectrum of TS-1; (b) Experimental HYSCORE spectrum of reduced TS-1 recorded at a magnetic field position corresponding to the arrow in spectrum (a); (c) Computer simulation of ^{14}N HYSCORE signals showed in the experimental spectrum (b); (d) Experimental (solid line) and simulated (dotted line) X-band CW-EPR spectrum of TiAlPO-5; (e) Experimental HYSCORE spectrum of reduced TiAlPO-5 recorded at a magnetic field position corresponding to the arrow in spectrum (d); (f) Computer simulation of ^{14}N HYSCORE signals detected in the experimental spectrum (e). CW EPR spectra were recorded at T = 77 K, while HYSCORE spectra at T = 10 K and τ value 172 ns. The simulated ^{14}N

HYSCORE spectra were obtained with the spin Hamiltonian parameters reported in Table 1. In the inset of spectrum (e) the ^{1}H HYSCORE spectrum plotted at low contour level is reported. Spectra taken at other magnetic field settings are reported as Supporting Information

A ^{1}H signal due to the coordinated ammonia protons is observed in both cases. Due to suppression effects[50] associated to the deep modulation depth of the TiAlPO-5 case, where at least two ^{14}N nuclei are interacting with the unpaired electron, the proton signal shows a reduced intensity. The signal is shown in the inset of Figure 5e plotted at a lower contour level with respect to the ^{14}N signals.

The spin-Hamiltonian parameters for the N interaction are reported in Table 2 for both TS-1 and TiAlPO-5. The isotropic hyperfine coupling $|A_{iso}|$ = 4.6 MHz derived from simulation is of the same order of that of TiAlPO-5 ($|A_{iso}|$ = 4.1 MHz) and corresponds to a spin density population in the N 2*s* orbital (a_0 = 1540 MHz)[43] of ≈0.3%. This value is comparable to that observed for amino nitrogens axially ligated to Ti^{3+} in the [1-{2-(*t*-butyl)-2-sila-2,2-dimethyl}-2,3,4,5-tetramethylcyclopentadienyl]-methyl titanium (III) complex.[51] Similar values were also reported for coordination of ammonia to vanadyl sites of vanadium silicate-1 nanoparticles deposited in SBA-15[52]and ZSM-5 zeolites[53] and are also comparable with values found for nitrogens equatorially bound to an oxo-vanadiumcation, VO^{2+},[54]characterized by a d^1 ground state with the unpaired electron in the d_{xy} orbital. From the HYSCORE simulation it emerges that the two N nuclei share the same hyperfine coupling constants and relative orientations (Table 2) suggesting that the two ammonia molecules are symmetrically coordinated in an axial position.[33b] This coordination mode should however be tested against DFT modelling.

Table 2. Spin-Hamiltonian parameters of $^{14}NH_3$ coordinated to Ti^{3+} centers. All hyperfine and quadrupole coupling constants are given in MHz. Euler angles are given in degrees.

System	g_1	g_2	g_3	$\|A_1\|$ ±0.2	$\|A_2\|$ ±0.2	$\|A_3\|$ ±0.2	α,β,γ ±10	$\|e^2qQ/h\|$ ±0.2	η ±0.1	α',β',γ' ±10
	1.90±0.01	1.949±0.001	1.965±0.005							
TS-1	1.91±0.02	1.970±0.01	1.981±0.002	3.4	4.6	5.8	0, 80, 20	2.7	0.1	0, 10, 30
	1.922±0.005	1.939±0.005	1.990±0.001							
TiAlPO-5	1.895±0.006	1.913±0.006	1.946±0.001	3.5	3.9	4.8	0, 90, 30	2.8	0.1	0, 40, 60

The most intriguing fact that emerges from the ^{14}N HYSCORE spectra of adsorbed ammonia is the preference towards 5-fold coordination in TS-1 with respect to TiAlPO-5. The situation is schematically illustrated in Scheme 1b. In the reduced TiAlPO-5 system, which also features tetrahedrally coordinated Ti^{3+} unambiguous evidence was obtained for the coordination of at least two ammonia molecules via the presence of distinct combination peaks in the ^{14}N HYSCORE spectrum.[33] Being the Ti^{3+} ions structurally

equivalent, as also testified by the similarity of the **g** tensors extracted from the CW-EPR spectra, the difference in the chemical reactivity of the two species has to be found in the different nature of the two matrixes. One possible explanation is to consider the different ionic character of the two frameworks. Corà and Catlow[26] have shown by population and topological analyses of the calculated electronic density that the bonding in AlPOs is of molecular−ionic character and comprised of discrete Al^{3+} and PO_4^{3-} ions. On the other hand a continuum semi-covalent network is the distinctive feature of the silica structure. The ionicity of the Al−O interaction compared to the covalent Si−O backbone may explain the different behavior towards NH_3 ligation of the substituted Ti in the silicalite and AlPO-5 frames allowing for a larger distortion in the case of the more ionic solid. The coordination of two NH_3 molecules requires a pronounced re-arrangement of the local framework structure, which indeed is relatively easy in the case of an ionic system. Another possible explanation is to consider the different chemistry of phosphorous with respect to silicon and in particular the capability of forming a P=O double bond, providing an extra coordinating vacancy. At this stage we are not in the position to discriminate between the two possibilities. We remark that in any case this is the first time that the nature of the matrix can be directly linked to the different chemical reactivity of isomorphously substituted TM ion.

5. Conclusions

In summary, we have reported an overview of EPR results relative to the characterization of the structure and chemistry of titanium ions doped into different microporous heterogeneous catalysts, highlighting the potential of advanced EPR techniques in the elucidation of the catalytic behavior of discrete and well-defined active sites in porous architectures. The redox activity and coordination symmetry are probed via CW EPR experiments, while HYSCORE experiments provide crucial insights into the local environment and coordination chemistry of the Ti^{3+} species. The observation of well resolved superhyperfine interactions with magnetically active framework ions provides a compelling evidence for framework substitution of transition metal ions and allows identifying specific active sites. Pseudo-in situ reactions with gaseous molecules (NH_3) allowed to determine the chemical accessibility and coordination chemistry of the active sites, revealing a remarkable dependency of the Ti^{3+} coordination ability as a function of the chemical nature of the framework. The conventional continuous wave EPR technique will undoubtedly remain the mainstay in heterogeneous catalysis, thanks to the possibility

of reproducing experimental conditions close to those of industrial processes. However integration of standard EPR with advanced methods appears to be a valuable way to afford a fundamental understanding of the mechanistic characteristics, at the atomic scale, that can lead to the rational design and development of the new generation of highly active and selective catalysts.

Acknowledgements

This work is part of the research program of the Dutch Polymer Institute (DPI), project nr. 754.

References

[1] Adrian FJ (1968) J Colloid Interface Sci 26:317-354
[2] Lunsford JH (1972) Adv Catalysis 32:265-277
[3] Howe RF (1993) Colloids and Surfaces A: Physicochem. Eng. Aspects 72: 353-363
[4] Che M, Giamello E (1994)Catalyst Characterization: Physical Techniques for Solid Materials. Imelik B and Vedrine JC (Eds.) Ch. 6
[5] Dyrek K, Che M (1997) Chem Rev 97:305-331
[6] Chiesa M, Giamello E, Che M (2010) Chem Rev 110:1320-1347
[7] Bruckner A (2010) Chem Soc Rev 39:4673-4684
[8]Van Doorslaer S, Murphy DM (2012) EPR Spectroscopy in Catalysis, Topics in Current Chemistry 321, 1-39
[9] Goldfarb D (2006) Phys Chem Chem Phys 8:2325-2343
[10] a) Dinse A, Ozarowski A, Hess C, Schomäcker R, Dinse KP (2008) J Phys Chem C 112:17664-17671; b) Dinse A, Carrero C, Ozarowski A, Schomäcker R, Schlögl R, Dinse KP (2012) Chem Cat Chem 4:641-652; c) Dinse A, Wolfram T, Carrero C, Schlögl R, Schomäcker R, Dinse KP (2013) J Phys Chem C 117:16921-16932; d) Pöppl A, Manikandan P, Köhler K, Maas P, Strauch P, Böttcher R, Goldfarb D (2001) J Am Chem Soc 123:4577-4584
[11] Raja R, Potter ME, Newland SH (2014) Chem Commun 50:5940-5957
[12] a) Taramasso M, Perego G, Notari B (1983) US Patent nr. 4410501; b) Notari B (1996) Adv Catal 41:253-334
[13] Wilson SI, Lok BM, Messina CA, Cannan TR, Flanigen EM (1982) J Am Chem Soc104:1146-1147
[14] a) Lee SO, Raja R, Harris KDM, Thomas JM, Johnson BFG, Sankar G (2003) Angew Chem Int Ed 42:1520-1523; b) Raja R, Sankar G, Thomas JM (1999) J Am Chem Soc 121:11926-11927; c) Thomas JM, Raja R, Sankar G, Bell RG (2001) Acc Chem Res 34:191-200
[15] Arends I W C E, Sheldon RA, Wallau M, Schuchardt U (1997) Angew ChemInt Ed Engl 36:1144-1163
[16] Oldroyd RD, Sankar G, Thomas JM, Ozkaya D (1998) J PhysChem B 102:1849-1855
[17] a) Notari B (1996) AdvCatal41:253-334; b) Tanev PT, Chibwe M, Pinnavaia TJ (1994) Nature 368:321-323; c) Anpo M, Thomas JM (2006) Chem Commun 3273-3278; d) Paterson J, Potter M, Gianotti E, Raja R (2011)Chem Commun 47:517-519
[18] Corma A, Navarro MT, Pérez Pariente J (1994) J Chem Soc Chem Commun 147-148
[19] Oldroyd RD, Thomas JM, Maschmeyer T, Mac Faul PA, Snelgrove DW, Ingold KU, Wayner DDM (1996) Angew Chem Int Ed Engl 35:2787-2790
[20] Maschmeyer T, Rey F, Sankar G, Thomas JM (1995) Nature 378:159-162
[21] Gianotti E, Dellarocca V, Marchese L, Martra G, Coluccia S, Maschmeyer T (2002) Phys Chem Chem Phys 4-6019-6115
[22] Anpo M, Thomas JM (2006) Chem Commun 31:3273-3278
[23] Thomas JM, Raja R, Lewis DW (2005) Angew Chem Int Ed 44:6456-6482
[24] Zhanpeisov NU, Anpo M (2004) J Am Chem Soc126:9439-9444
[25] Bordiga S, Bonino F, Damin A, Lamberti C (2007) Phys Chem Chem Phys 9:4854-4858

[26] Corà F, Catlow CRA (2001) J Phys Chem B 105:10278-10281
[27] a) Kuznicki SM (1989) US Patent nr. 4853202; b) Anderson MW, Terasaki O, Ohsuna T, Philippou A, Mac Kay SP, Ferreira A, Rocha J, Lidin S (1994) Nature 367:347-351
[28] a) Philippou A, Naderi M, Rocha J, Anderson MW (1998) Catal Lett 53:221-224; b) Philippou A, Anderson MW (2000) J Catal 189:395-400; c) Valente A, Lin Z, Brandão P, Portugal I, Anderson MW, Rocha J (2001) J Catal 200:99-105; d) Doskocil EJ (2005) J Phys Chem B 109:2315-2320; e) Waghmode SB, Vetrivel R, Gohinath CS, Sivasanker S (2004) J Phys Chem B 108:11541-11548
[29] a) Borello E, Lamberti C, Bordiga S, Zecchina A, Areán CO (1997) Appl Phys Lett 71:2319-2321; b) LlabrésiXamena FX, Damin A, Bordiga S, Zecchina A (2003) Chem Commun 1514-1515; c) Damin A, LlabrésiXamena FX, Lamberti C, Civalleri B, Zicovich-Wilson CM, Zecchina A (2004) J Phys Chem B 108:1328-1336; d) Bordiga S, Palomino GT, Zecchina A, Ranghino G, Giamello E, Lamberti C (2000) J Chem Phys 112:3859-3867
[30] Goodenough JB (1971) Progress in solid state chemistry Pergamon, NewYork
[31] Ricchiardi G, Damin A, Bordiga S, Lamberti C, Span G, Rivetti F, Zecchina A (2001) J Am Chem Soc 123:11409-11419
[32] Gallo E, Bonino F, Swarbrick JC, Petrenko T, Piovano A, Bordiga S, Gianolio D, Groppo E, Neese F, Lamberti C, Glatzel P (2013) Chem Phys Chem 14:79-83
[33] a) Maurelli S, Muthusamy V, Chiesa M, Berlier G, Van Doorslaer S (2011) J Am Chem Soc 133:7340-7343; b) Maurelli S, Vishnuvarthan M, Berlier G, Chiesa M (2012) Phys Chem Chem Phys 14:987-995; c) Novara C, Alfayate A, Berlier G, Maurelli S, Chiesa M (2013) Phys Chem Chem Phys 15:11099-11105
[34] Höfer P, Grupp A, Nebenfür H, Mehring M (1986) Chem Phys Lett 132:279-282
[35] Stoll S, Schweiger A (2006) J Magn Reson 178:42-55
[36] Prakash AM, Kevan L (1998) J Catal 178:586-597
[37] Morra E, Giamello E, Chiesa M (2014) Chem Eur J 20:7381-7388
[38] Figgis BN (1967) Introduction to Ligand Fields. John Wiley & Sons, New York
[39] Weil JA, Bolton JR, Wertz JE (1994) Electron Paramagnetic Resonance: Elementary Theory and Practical Applications. John Wiley, New York
[40] Abraham A, Bleaney B (1970) Electron Paramagnetic Resonance of Transition Ions. Oxford University Press, Oxford
[41] Solntsev VP, Yurkin AM (2000) Cryst Reports 45:128-132
[42] Maurelli S, Livraghi S, Chiesa M, Giamello E, Van Doorslaer S, Di Valentin C, Pacchioni G (2011) Inorg Chem 50:2385-2394
[43] Zamani S, Meynen V, Hanu AM, Mertens M, Popovici E, Van Doorslaer S, Cool P (2009) Phys Chem Chem Phys 11:5823-5832
[44] Fitzpatrick JAJ, Manby FR, Western CM (2005) J Chem Phys 122:084312-1-12
[45] Arieli D, Delabie A, Strohmaier KG, Goldfarb D (2002) J Phys Chem B 106:7509-7519
[46] a) Maurelli S, Chiesa M, Giamello E, Leithall R M, Raja R (2012) Chem Commun 48: 8700-8702; b) Leithall R, Shetti V, Maurelli S, Chiesa M, Gianotti E, Raja R (2013) J Am Chem Soc 135: 2915-2918
[47] Maurelli S, Berlier G, Chiesa M, Musso F, Corà F (2014) J Phys Chem C 118:19879-19888
[48] a) Kataev V, Baier J, Moller A, Jongen L, Meyer G, Freimuth A (2003) Phys Rev B 68:140405-1-4; b) Ruckamp R, Baier J, Kriener M, Haverkort MW, Lorenz T, Uhrig GS, Jongen L, Möller A, Meyer G, Grüninger M (2005) Phys Rev Lett 95:097203-1-4; c) Krimmel A, Strempfer J, Bohnenbuck B, Keimer B, Hoinkis M, Klemm M, Horn S, Loidl A, Sing M, Claessen R, Zimmermann MV (2006) Phys Rev B 73:172413-1-4; d) Law JM, Hoch C, Glaum R, Heinmaa I, Stern R, Kang J, Lee C, Whangbo MH, Kremer RK (2011) Phys Rev B 83:180414-1-4
[49] Dikanov SA, Tsvetkov YD, Bowman MK, Astashkin AV (1982) Chem Phys Lett 90:149-153
[50] Stoll S, Calle C, Mitrikas G, Schweiger A (2005) J Magn Reson 177:93-101
[51] Van Doorslaer S, Shane JJ, Stoll S, Schweiger A, Kranenburg M, Meier RJ (2001) Organomet Chem 634:185-192
[52] Zamani S, Chiesa M, Meynen V, Xiao Y, Prélot B, Zajac J, Verpoort F, Cool P, Van Doorslaer S (2010) J Phys Chem C 114:12966-12975
[53] Woodworth J, Bowman MK, Larsen SC (2004) J Phys Chem B 108:16128-16134
[54] a) Fukui K, Ohya-Nishigchi H, Kamada H (1997) Inorg Chem 36:5518-5529; b) Buy C, Matsui T, Andrianambinintsoa S, Sigalat C, Girault G, Zimmermann JL (1996) Biochemistry 35:14281-14293; c) Fukui K, Ohya-Nishigchi H, Kamada H, Iwaizumi M, Xu Y (1998) Bull Chem Soc Jpn 71:2787-2796; d) Dikanov SA,

Tyryshkin AM, Huttermann J, Bogumil R, Witzel H (1995) J Am Chem Soc 117:4976-4986; e) Dikanov SA, Samoilova RI, Smieja JA, Bowman MK (1995) J Am Chem Soc 117:10579-10580; f)Mulks CF, Kirste B, Van Willigen H, Bowman MK (1982) J Am Chem Soc 104:5906-5911; g) Kirste B, Van Willigen H (1982) J Phys Chem 86:2743-2753